
Article:
Slattery, John Martin orcid.org/0000-0001-6491-8302, Smoll, Eric J., Tesa-Serrate, Maria A. et al. (6 more authors) (2017) Determining the Composition of the Vacuum-Liquid Interface in Ionic-Liquid Mixtures. FARADAY DISCUSSIONS. ISSN 1364-5498

https://doi.org/10.1039/C7FD00175D

Faraday Discussions

Accepted Manuscript

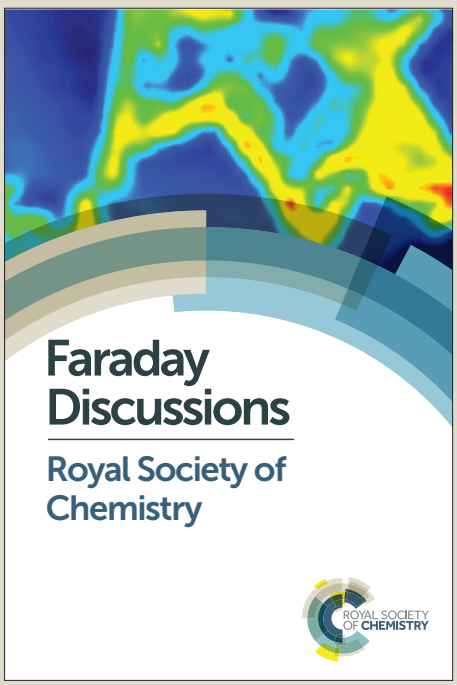

This article can be cited before page numbers have been issued, to do this please use: E. Smoll, M. T. Serrate, S. Purcell, L. D'Andrea, D. W. Bruce, J. M. Slattery, M. Costen, T. Minton and K. G. McKendrick, *Faraday Discuss.*, 2017, DOI: 10.1039/C7FD00175D.

Faraday Discussions

View Article Online
DOI: 10.1039/C7FD00175D

ARTICLE

Determining the Composition of the Vacuum-Liquid Interface in Ionic-Liquid Mixtures

Received 00th January 20xx,
Accepted 00th January 20xx

DOI: 10.1039/x0xx00000x

www.rsc.org/

E. J. Smoll Jr.,[a] M. A. Tesa-Serrate,[b] S. M. Purcell,[b] L. D'Andrea,[c] D. W. Bruce,[c] J. M. Slattery,[c] M. L. Costen,[b] T. K. Minton[a] and K. G. McKendrick[b]

The vacuum-liquid interfaces of a number of ionic-liquid mixtures have been investigated using a combination of reactive-atom scattering with laser-induced fluorescence detection (RAS-LIF), selected surface tension measurements, and molecular dynamics (MD) simulations. The mixtures are based on the widespread 1-alkyl-3-methylimidazolium ($[C_n mim]^+$) cation, including mixed cations which differ in chain length or chemical functionality with a common anion; and different anions for a common cation. RAS-LIF results imply that the surface compositions exhibit a general form of non-stoichiometric behaviour that mimics the well-known Henry's and Raoult's laws at low and high mole fraction, respectively. The Extended Langmuir model provides a moderately good single-parameter fit, but higher-order terms are required for an accurate description. The quantitative relationship between RAS-LIF and surface tension, which probes the surface composition only indirectly, is explored for mixtures of $[C_2mim]^+$ and $[C_{12}mim]^+$ with a common bis(trifluoromethylsulfonyl)imide ($[NTf_2]^-$) anion. Extended Langmuir model fits to surface tension data are broadly consistent with those to RAS-LIF; however, several other common approaches to extracting surface compositions from measured surface tensions result in much larger discrepancies. MD simulations suggest that RAS-LIF faithfully reports on the alkyl-chain exposure at the surface, which is only subtly modified by composition-dependent structural reorganisation.

…

Introduction

A substantial amount of scientific effort has been expended over the last 20 years or so in the discovery and exploration of the properties of room-temperature ionic liquids (ILs).[1-3] As amply evidenced elsewhere in this volume, the search for the most suitable ILs for specific applications remains a highly active area.[4] Among these applications, a number are critically affected by the surface properties of the liquid. The more obvious examples include gas sequestration and separation; and multiphase catalysis.[5-10]

The nature of the surface layer is an interesting and non-trivial question for ILs because of the inherent chemical heterogeneity of the components. Nanoscale segregation in the bulk into polar and non-polar domains is commonplace, particularly in ILs with hydrophobic alkyl substituents on either the cation or anion.[11] The question of how these extended structures terminate at the gas-liquid (or vacuum-liquid) interface, and how this depends on the chemical structure of the IL, is therefore of considerable interest.

It is natural therefore that attempts have been made to investigate the interfacial properties of ILs using a range of physical methods. The most ubiquitous approach is the classical measurement of surface tension.[12] However, this is subject to the fundamental limitation that the interfacial composition can only be inferred indirectly. Alternatively, an array of other, more direct, surface-analysis techniques have relatively recently begun to be applied to IL surfaces, enabled by the very low vapour pressures of many ILs of practical interest. The most prominent among them include angle-resolved X-ray photoelectron spectroscopy (ARXPS),[13, 14] high-resolution Rutherford backscattering (HRBS),[15] secondary-ion mass spectrometry (SIMS)[15] and low-energy ion scattering (LEIS).[16] Distinct non-linear optical approaches have also been exploited successfully, particularly second harmonic generation (SHG) and sum frequency generation (SFG) spectroscopies.[17]

[a] Department of Chemistry and Biochemistry, Montana State University, Bozeman, Montana 59717, USA.
[b] Institute of Chemical Sciences, School of Engineering and Physical Sciences, Heriot-Watt University, Edinburgh, EH14 4AS, United Kingdom
[c] Department of Chemistry, University of York, Heslington, York YO10 5DD, United Kingdom
† Footnotes relating to the title and/or authors should appear here.
Electronic Supplementary Information (ESI) available: Ionic liquid synthesis and characterization; surface tension measurements; RAS-LIF rotational distributions and appearance profiles; integrated RAS-LIF OH density and relative surface exposure values; fitting procedural details. See DOI: 10.1039/x0xx00000x

View Article Online
DOI: 10.1039/C7FD00175D

These various direct measures are all subject to some degree to a finite penetration depth (hence lack of true surface-selectivity), or lack of chemical specificity, or both.[14, 16-18] Complementing the established techniques, we have developed an alternative approach based on reactive-atom scattering (RAS), combined either with mass spectrometric (RAS-MS) or laser-induced fluorescence (RAS-LIF) detection.[18-26] The essence of this method, of which the RAS-LIF variant is the one we use here, is that projectiles interrogate the liquid surface via selective reaction with specific functional groups, producing a gas-phase product which is detected quantitatively. The dynamical attributes of these products confirm that they originate in the extreme outer layers of the liquid.[18, 25]

Based on results obtained using this array of techniques, there is general consensus for single-component ILs composed of a single cation-anion pair that the outer surface is increasingly dominated by hydrophobic alkyl chains as the chain length increases. In contrast, the surface properties of mixtures of ILs have been much less explored. These are attractive for potential applications because the properties can be fine-tuned by simply varying the mixing ratio, rather than having to synthesize a large number of chemically distinct compounds. Their surface properties have begun to be examined by direct techniques,[13, 15, 27-30] but the data remain relatively sparse. In particular, there have been no systematic attempts to investigate the relationships between these direct measures and the more-established but indirect measurement of surface tensions.

Addressing the relationships between different approaches to determining the surface composition of ionic-liquid mixtures is the aim of this paper. We focus on ILs based on the common [1-alkyl-3-methylimidazolium] cation (abbreviated to $[C_nmim]^+$). The mixture of $[C_2mim]$ bis(trifluoromethylsulfonyl)imide (abbreviated as $[NTf_2]^-$) and $[C_{12}mim][NTf_2]$, with distinct cationic alkyl chain lengths and a common anion, is selected as the primary system on which the fullest comparison is carried out; this is aided by the partial information using RAS-LIF and other direct measures (HRBS and TOF-SIMS), and complementary realistic molecular dynamics (MD) simulations, that are previously available.[15, 27, 29] However, we also include RAS-LIF data on $[C_8mim][NTf_2]$ mixed with an analogue containing a $C_2H_4(CF_2)_5CF_3$ fluorinated alkyl chain, $[C_8mimF_{13}][NTf_2]$, representing different chemical functionalities for chains of the same length; and $[C_6mim][BF_4]$ / $[C_6mim][NTf_2]$ mixtures of anions with a common cation, to illustrate the generality of the deviations from ideality that we observe. We examine for the first time the level of complexity needed in empirical models to fit successfully the surface compositions determined by RAS-LIF. These observations are used to test different theoretical models that aim to predict the surface composition using only the surface tensions of the pure components, measured here as required, as input. The success or otherwise of a number of distinct approaches to recovering the surface composition from new measurements of surface tension across the full range of compositions is established. Ultimately, we answer the question of whether RAS-LIF and surface tension provide compatible measures of the surface composition, and whether these are consistent with the molecular-level picture provided by an extended analysis of MD simulations.

Methods

Materials

Figure 1 shows the molecular structure of the three IL mixtures used in this study. The $[C_2mim]_{(1-x)}[C_{12}mim]_x[NTf_2]$ and $[C_8mim]_{(1-x)}[C_8mimF_{13}]_x[NTf_2]$ mixtures, where x is a bulk mole fraction, and the corresponding neat ILs were synthesised as part of this work. The neat ILs for the anion mixtures, $[C_6mim][NTf_2]_x[BF_4]_{(1-x)}$, were purchased and used as received from IoLiTec (Germany). Details of the IL syntheses are provided in the electronic supplementary information (ESI), along with water and halide content for the commercial ILs. The RAS-LIF measurements also used a reference liquid, the branched-chain hydrocarbon, squalane (2,6,10,15,19,23-hexamethyltetracosane) which was used as supplied by Aldrich (99 %). Prior to experiment, the ILs and squalane were degassed overnight under high vacuum to minimise water, or other volatile, content.

View Article Online
DOI: 10.1039/C7FD00175D

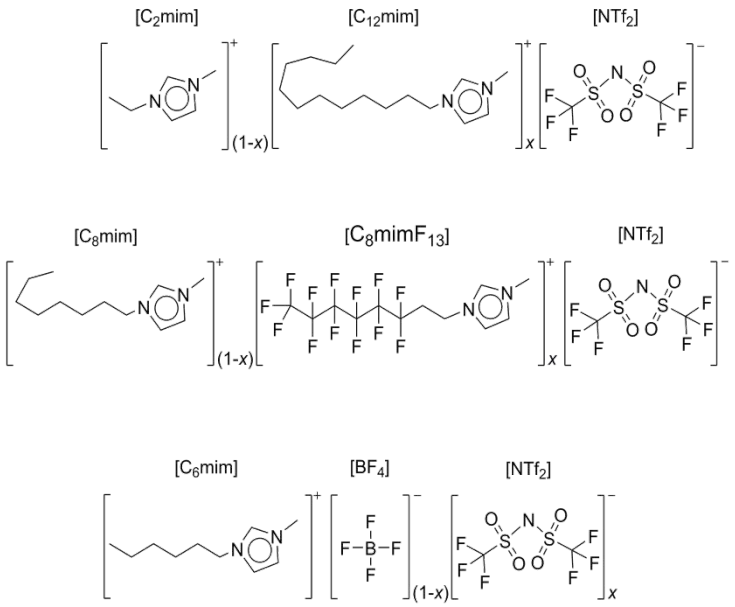

Figure 1: Chemical structures and abbreviated nomenclature of the ionic liquid mixtures studied in this work.

Experimental

Surface tension measurements

Surface tension measurements of the pure $[C_2mim][NTf_2]$ and $[C_{12}mim][NTf_2]$ ILs and their mixtures, and of pure $[C_8mim][NTf_2]$ and $[C_8mimF_{13}][NTf_2]$, were performed at 296 K under atmospheric pressure with a Krüss DSA100 tensiometer, using drop-shape-analysis software. In all cases eight or more successive measurements were carried out, obtaining standard deviations in the range 0.03-0.49 $mN{\cdot}m^{-1}$. Measurements of the surface tension of Milli-Q water at 296 K were performed to calibrate the pendant drop tensiometer. For all measurements, disposable needles of inner diameter 1.820 mm were used. The manufacturer´s specified resolution and accuracy for this instrument is 0.01 $mN{\cdot}m^{-1}$and 0.3 $mN{\cdot}m^{-1}$, respectively.

Reactive atom scattering

The RAS-LIF approach and the details of the apparatus have been described in detail elsewhere.[18, 24, 26] Fig. 2 shows schematically the basis of the approach. The reactive atoms, in this case $O(^3P)$, are generated by laser photolysis of a low-pressure (1 mTorr) precursor gas (NO_2) above the liquid surface. A continually refreshed surface was generated in the now-conventional manner by using a rotating wheel (diameter 5 cm) immersed in a temperature-controlled bath of the liquid. All measurements were made with the multiple-wheel assembly indicated in Fig. 2, which importantly allows accurate comparisons of the signals from different liquids without breaking the vacuum.[24]

View Article Online
DOI: 10.1039/C7FD00175D

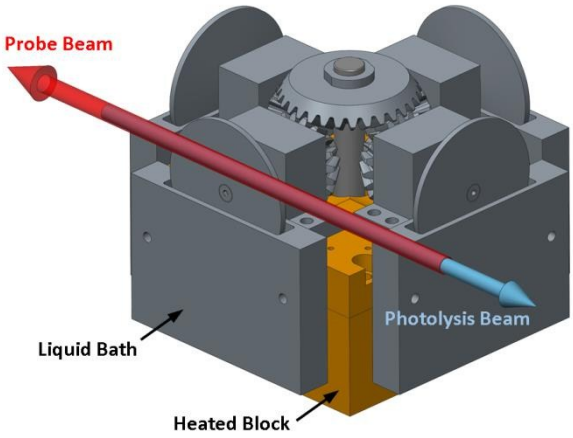

Figure 2: Schematic representation of the multi-wheel assembly and laser beams used in the collection of RAS-LIF data.

Photolysis of NO_2 at 355 nm generates O-atoms with a laboratory-frame translational energy distribution with an average of 16 kJ mol^{-1} and a spread of 26 kJ mol^{-1} (FWHM).[31] This is important because it influences strongly the types of C-H from which H-atoms can be abstracted to form the observed product, OH. As explained in detail elsewhere,[23, 24] in all mixtures considered here the only significant contribution to the OH yield will come from secondary aliphatic C-H bonds in the pendant alkyl chain on the imidazolium headgroup.

The OH radical products that scattered back into the vacuum were excited on the A-X band by a probe laser pulse which counter-propagated with respect to the photolysis laser along the same axis. The fluorescence signal was collected by suitable optics and detected using a photomultiplier tube (PMT).

The experiment was operated in two modes. LIF excitation spectra were recorded by scanning the probe-beam wavelength at a fixed delay between the photolysis and probe pulses. These are not the main focus here, but were necessary to confirm that the observed yields from different liquids were not biased by different OH rotational populations. The principal data presented here are derived from appearance profiles, where the intensity of the OH LIF signal was recorded on a fixed transition as a function of delay between the photolysis and probe pulses. For all liquids, appearance profiles were recorded on the most intense, $Q_1(1)$, line. Signal sizes were referenced against interleaved measurements of the well-studied standard, squalane.[32-40] To achieve the desired precision, the appearance profiles were averaged over typically ten sets of independent measurements over several different days for each mixture studied. They were corrected for a small background signal caused by a HONO impurity in the chamber by the procedure described previously.[23, 24]

A temperature-controlled circulator was used to regulate the temperature of liquid samples held in the carousel. Due to the increased viscosity of $[C_8mimF_{13}][NTf_2]$ compared to $[C_8mim][NTf_2]$, all measurements of $[C_8mim]_{(1-x)}[C_8mimF_{13}]_x[NTf_2]$ were conducted at 46±2 °C, to allow a good quality liquid film to form on the wheel. All other IL mixture measurements were conducted at 22±2 °C. Extensive previous measurements have shown that the OH yield from related ILs is only very weakly dependent on liquid temperature.[26]

Molecular dynamics simulations

To complement the experiment, we analysed realistic models of the $[C_2mim]_{(1-x)}[C_{12}mim]_x[NTf_2]$ vacuum-liquid interface generated by classical MD simulations. Simulation details are available in a recent publication.[27] Briefly, all MD calculations were performed with tools available in GROMACS 5.1.2.[41] All molecular interactions were described with the Canongia-Lopes and Pádua (CL&P)[42-48] additions to the OPLS-AA[49-56] forcefield. MD simulations were carried out under 3D periodic boundary conditions, smooth Particle-Mesh Ewald long-range electrostatics, 1.5 nm cutoffs, and a velocity-rescaling thermostat.[57]

In total, eight $[C_2mim]_{(1-x)}[C_{12}mim]_x[NTf_2]$ mixtures were studied where x = 0, 0.04, 0.08, 0.16, 0.24, 0.52, 0.87 and 1. Each mixture was initialized with a vacuum-liquid-vacuum slab structure within a 7.5 nm x 7.5 nm x 22.5 nm periodic-boundary-condition unit cell. The liquid slab of each mixture is approximately cubic with an edge length of 7.5 nm. To approach equilibrium, each mixture

was subjected to five sequential equilibration cycles, where an equilibration cycle is defined as 4-10 ns of NVT propagation at 500 K followed by 4-10 ns of NVT propagation at 298 K. All data analysis was performed on the final 10 ns trajectory at 298 K.

View Article Online
DOI: 10.1039/C7FD00175D

Number density distributions were calculated by dividing the unit cell along the z-axis into 400 equally-sized boxes. For each box, the trajectory-averaged number density of a specific cation-atom type is associated with the z-coordinate of the box centre. For improved statistics at the vacuum-liquid interface, all number density profiles were spatially-averaged about the z-coordinate of the liquid slab centre.

The conformation of surface-active $[C_{12}mim]^+$ dodecyl groups was also quantified by tracking the orientation of vectors defined between specific carbon atom pairs in the dodecyl chain. Surface-active dodecyl groups were selected by visual inspection. For dodecyl-group vectors at the upper (lower) vacuum-liquid interface, the angle, θ, between each vector and the positive (negative) z-axis was computed and collected in a histogram that sums over all frames of the analysis trajectory. Probability distribution profiles were computed from these histograms by normalizing each bin value by the unit-sphere surface area spanned by the bin range.

Experimental Results

Surface tension

Table 1 shows the surface tension measurements for the neat ionic liquids in this work. Surface tensions for $[C_6mim][NTf_2]$ and $[C_6mim][BF_4]$ were taken from previous work.[58] The results for the pure components compare favourably (within ±0.7 mN m^{-1} for $[C_2mim][NTf_2]$ and $[C_8mim][NTf_2]$, and 0.1 mN m^{-1} for $[C_{12}mim][NTf_2]$, when scaled to 298.15 K) with previous measurements.[12, 59] Consistent with many previous measurements on related single-component ILs with different chain lengths,[12] the surface tension of pure $[C_{12}mim][NTf_2]$ is lower than that of $[C_2mim][NTf_2]$. There are also marked differences in surface tension between the respective pairs $[C_8mim][NTf_2]$ / $[C_8mimF_{13}][NTf_2]$ and $[C_6mim][BF_4]$ / $[C_6mim][NTf_2]$.

Liquid	Surface Tension / mN m^{-1}	Temperature / K
$[C_2mim][NTf_2]$	35.2	296
$[C_{12}mim][NTf_2]$	29.8	296
$[C_8mim][NTf_2]$	30.4	296
$[C_8mimF_{13}][NTf_2]$	21.9	296
$[C_6mim][BF_4]$	36.8[a]	298.15
$[C_6mim][NTf_2]$	32.5[a]	298.15

Table 1: Surface tensions for neat ionic liquids whose mixtures are investigated in this work. Results are from this work unless otherwise indicated. [a]Reference [58].

The measured surface tensions of $[C_2mim]_{(1-x)}[C_{12}mim]_x[NTf_2]$ mixtures for a series of compositions are shown in Figure 3. The new but also not unexpected result reported here is that there is a general deviation towards lower surface tension than expected from stoichiometry (diagonal line). This has also been observed previously for related systems.[60, 61]

RAS-LIF

Figure 4 shows representative averaged appearance profiles for $[C_8mim]_{(1-x)}[C_8mimF_{13}]_x[NTf_2]$ mixtures of multiple bulk compositions. Excitation spectra recorded at the peak of the appearance profiles [see ESI] confirmed that no significant bias was introduced by different rotational populations from different liquids. Within each mixture system studied, the appearance profiles have essentially the same distribution of arrival times, meaning the average OH velocities are the same and no density-flux correction is required. The appearance profiles were integrated directly and normalised to the integrated squalane profile; the resulting integral value is termed 'reactivity' and is, within known limitations, directly related to the exposure of secondary alkyl chains at the liquid surface.[23]

Essentially the same process of measuring appearance profiles was carried out for the $[C_2mim]_{(1-x)}[C_{12}mim]_x[NTf_2]$ mixtures[27] and for $[C_6mim][NTf_2]_x[BF_4]_{(1-x)}$ (shown in the ESI). The processed results of reactivity as a function of mole fraction are collected in Fig. 5.

View Article Online
DOI: 10.1039/C7FD00175D

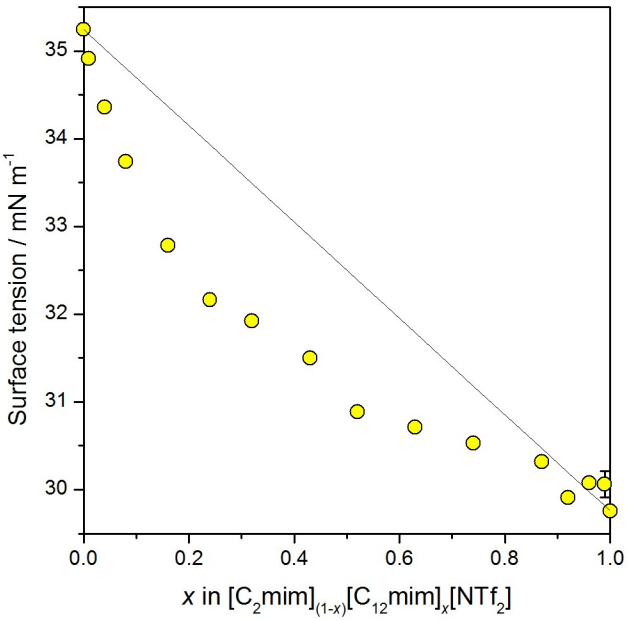

Figure 3: Surface tension plotted against bulk mole fraction, *x*, for $[C_2mim]_{(1-x)}[C_{12}mim]_x[NTf_2]$. Error bars smaller than the symbol are not shown; the remaining error bar is 1σ SEM.

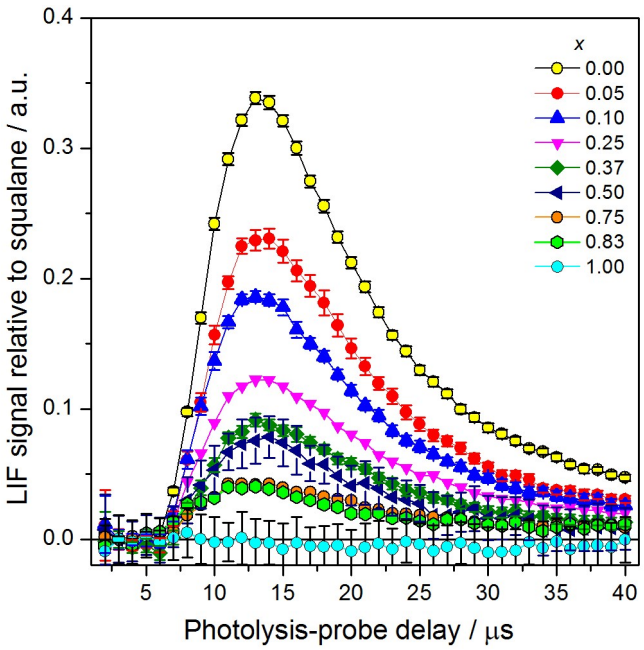

Figure 4: RAS-LIF OH appearance profiles from $[C_8mim]_{(1-x)}[C_8mimF_{13}]_x[NTf_2]$ mixtures for varying *x*. The magnitude of each appearance profile is shown as a fraction of the peak OH LIF signal from the reference liquid squalane. Error bars are 1σ SEM; errors smaller than the symbols have been omitted.

As we have previously established,[27] the C12 chain is preferentially at the surface in $[C_2mim]_{(1-x)}[C_{12}mim]_x[NTf_2]$. This can be seen directly from the universally higher yield of OH than predicted from stoichiometry (diagonal line) in Fig. 5a. Similarly, we establish here for the first time that the predominantly fluorinated C8 chain in $[C_8mim]_{(1-x)}[C_8mimF_{13}]_x[NTf_2]$ mixtures has the greater surface preference, from the corresponding yield of OH deviating strongly *below* the stoichiometric line in Fig. 5b. Note that pure $[C_8mimF_{13}][NTf_2]$ gives effectively zero OH yield, implying that the $–CH_2CH_2-$ linker unit between the perfluoroalkyl chain and the

ring N atom is either not significantly exposed or, in principle, has C-H bond strengths sufficiently affected by its chemical environment to suppress its reactivity within the constrained kinetic energy of the O(^{3}P) atoms.

View Article Online
DOI: 10.1039/C7FD00175D

Also demonstrated here for the first time, Fig. 5c shows that the OH yield from $[C_6mim][NTf_2]_x[BF_4]_{(1-x)}$ mixtures deviates below the line at low *x*. We infer from this that the $[NTf_2]^-$ ion is dominating the surface region, on the basis of our previous observations that the OH yield from $[C_nmim][NTf_2]$ single-component liquids is always systematically lower than from the corresponding $[C_nmim][BF_4]$ liquids.[23] We have rationalised this previously largely on the basis of ionic volume: in essence, the larger anion reduces the packing density of the cationic headgroups and hence of alkyl chains at the surface. Compatible results have been reported for systems based on the $[C_4mim]^+$ cation with mixed $[NTf_2]^-$ and halide or mixed $[BF_4]^-$ and $[HOSO_3]^-$ anions by Lovelock and co-workers using LEIS, and by Nakajima et al for $[C_2mim]^+$ with mixed $[NTf_2]^-$ and $[BF_4]^-$ anions by HRBS.[28, 30]

All three sets of results in Fig. 5 are consistent with the simple observation that the surface is dominated by the component with the lower surface tension (compare Table 1). Beyond the simple sense of this deviation, the generality that we are seeking to highlight in Figs. 5(a)-(c) is the immediate, near-linear departure of the OH yield from stoichiometry at low mole fraction of the more surface-active component. In contrast, at high *x*, to varying degrees but with a distinct inflexion in all cases, the behaviour returns towards the stoichiometric line as *x* approaches unity. Note that this also mimics the behaviour in the surface tension measurements in Fig. 2. The low *x* behaviour is the analogy of the very well-known Henry's Law for the more volatile component in a binary liquid mixture, while that at high *x* corresponds to Raoult's Law.

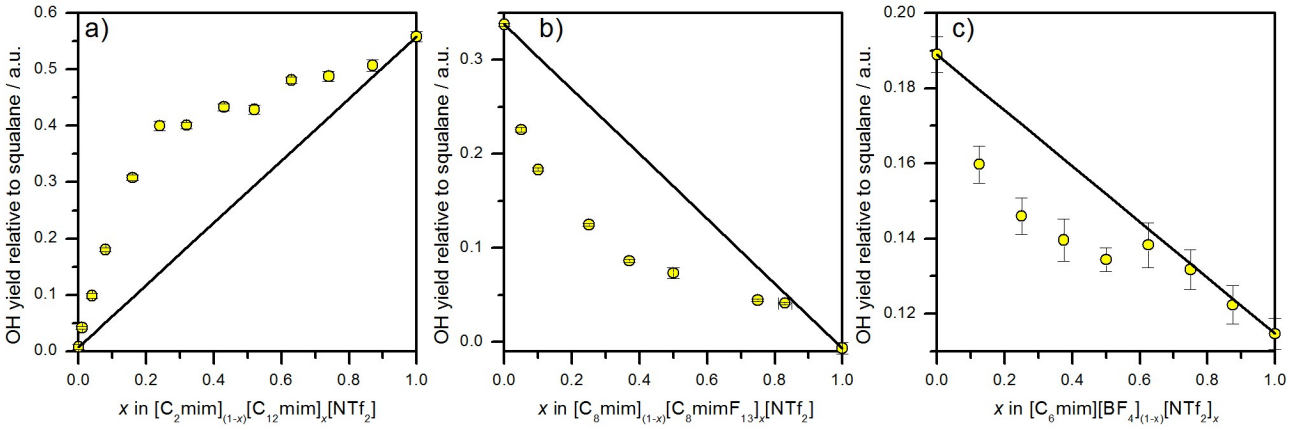

Figure 5: RAS-LIF OH yields from ionic liquid mixtures with a) cations with different alkyl chain lengths; b) cations with the same alkyl chain lengths but with a partially fluorinated alkyl chain; and c) different anion types. Error bars are 1σ SEM.

Analysis

Representation of the RAS-LIF data

The approaches taken by various authors differ in the preferred choice of independent variable. The bulk mole fractions, *x*, have the benefit of being simple and rigorously defined. However, they do not capture the simple physical fact that a bulkier ion is likely to occupy a larger area at the surface than a smaller one. Consequently, it is well-precedented to adopt the molar volume as the independent variable[62, 63] A third alternative is to use some measure of cross-sectional area. This can be challenging to define or estimate accurately, beyond some simplistic assumption of an approximately cubic (or, within a scaling factor, spherical) geometry; otherwise, an independent direct measure of the areal density is needed.[15, 29] We have shown previously that choosing either the area or the volume does not alter the qualitative form of the behaviour in plots such as those in Figure 5.[27] In what follows, we use these different independent variables appropriate to the basis on which the various expressions we will introduce have been developed.

The results in Fig. 4 and 5 are normalised to the internal reference, squalane. For the purposes of comparison with analytical predictions and the performance of fitting functions, we define *relative surface exposures* of components 1 and 2, denoted S_1 and S_2, respectively. We choose in all cases that component 2 is the one with the higher surface preference. The total observed OH yield, I_{OH}, is assumed to be a linear combination of the OH yields from the pure components, $I_{OH(1)}$ and $I_{OH(2)}$:

$$I_{OH} = S_1 I_{OH(1)} + S_2 I_{OH(2)} \qquad \textbf{(1)}$$

Note from Fig. 5(a) that for $[C_2mim]_{(1-x)}[C_{12}mim]_x[NTf_2]$ mixtures, $I_{OH(1)}$ is practically zero and hence simply, to a very good approximation with no further assumptions, $S_2 = I_{OH} / I_{OH(2)}$, i.e. the signal from the mixture normalised to that from pure $[C_{12}mim]_x[NTf_2]$. This result is independent of whether the surface exposures in the mixture sum to unity; in principle, they may not do so because there is no absolute constraint on the fraction of the true outer surface area occupied by the $[NTf_2]^-$ anion.

View Article Online
DOI: 10.1039/C7FD00175D

For mixtures such as $[C_8mim]_{(1-x)}[C_8mimF_{13}]_x[NTf_2]$ or $[C_6mim][NTf_2]_x[BF_4]_{(1-x)}$ in Figs. 5(b) and (c), respectively, where the OH LIF signal has a contribution (either totally, or in part) from component 1, it is necessary to assume that $S_1 + S_2 = 1$, allowing S_2 to be extracted from:

$$S_2 = \frac{I_{OH} - I_{OH(1)}}{I_{OH(2)} - I_{OH(1)}} \qquad \textbf{(2)}$$

As noted above, the significant differences in the cation / anion ratios at the surface of the pure $[C_6mim][BF_4]$ and $[C_6mim][NTf_2]$ materials are indirectly responsible for the relatively large overall change in OH yield from $x = 0$ to 1 in Fig. 5(c). However, if the cation / anion ratio does not vary linearly with mixing ratio then this would cause deviations from eqn (2).

Alternative direct measurements

We begin the comparison of our results with other work by considering previous attempts to measure the surface composition directly. As far as we are aware, the only one of our mixtures which has been examined quantitatively by another direct method is $[C_2mim]_{(1-x)}[C_{12}mim]_x[NTf_2]$, for which the single composition, $x = 0.5$, was analysed by HRBS by Nakajima et al as part of a survey of a variety of equimolar mixtures.[29] The observed surface mole fraction of $[C_{12}mim][NTf_2]$ was reported to be 0.66 ± 0.06. We have indicated this point in Fig. 6, where it can be seen to be slightly lower but in reasonable agreement with our RAS-LIF measurement of 0.76 ± 0.02 at the nearest measured point of $x = 0.52$. Using the same method, Nakajima et al had previously found[15] preliminary results of 0.6 ± 0.05 (later refined[29] to 0.67 ± 0.07, very similar to the result for $[C_{12}mim][NTf_2]$) and 0.18 ± 0.02 by HRBS for $x = 0.5$ and 0.1 in $[C_2mim]_{(1-x)}[C_{10}mim]_x[NTf_2]$ mixtures. They noted that these differed quantitatively from their TOF-SIMS measurements, which yielded significantly higher surface segregations of 0.83 ± 0.03 and 0.42 ± 0.04, for the same two mixtures.[15] We have also added these two TOF-SIMS points to Fig. 6. Notwithstanding the small differences in chain length, there is again reasonable qualitative agreement with our results, but with the TOF-SIMS now giving somewhat higher surface segregations.

Predictions based on surface tensions of pure components

In their earlier work,[15] Nakajima et al attempted to reproduce their measured surface mole fractions via an early expression originally due to Guggenheim.[64] This model is based on statistical thermodynamic arguments, and formulated in terms of surface free energies per ion pair. It leads to the expression

$$x_2^s = \frac{x_2 \exp(-f_2 / kT)}{(1-x_2)\exp(-f_1 / kT) + x_2 \exp(-f_2 / kT)} \qquad \textbf{(3)}$$

where x_i^s is the mole fraction of component i at the surface. The surface free energies, f_1 and f_2, were derived by Nakajima et al. from the product of the independently measured surface tensions, σ_1 and σ_2, of the pure materials and the surface areas, A_1 and A_2, occupied by each ion-pair type. These areas could be estimated simply from bulk densities with an assumption of cubic geometry, or ostensibly more accurately from the observed areal atomic densities in their HRBS experiments.[15]

Using Nakajima et al's most recent surface-area estimates[29] and our own measured surface tensions for $[C_2mim]_{(1-x)}[C_{12}mim]_x[NTf_2]$ mixtures above, the dependence of surface mole fraction on bulk mole fraction shown in Fig. 6 is predicted, where it is compared with our RAS-LIF measurements of surface exposure. The level of agreement is not materially affected by modest changes in the estimated areas or alternative measurements of surface tension for the pure materials. It can be seen that the behaviour at low x is reproduced reasonably well, where the initial strong positive deviation from stoichiometry is captured. However, the more rapid observed decline towards stoichiometry at higher x in the RAS-LIF data is not successfully predicted.

View Article Online
DOI: 10.1039/C7FD00175D

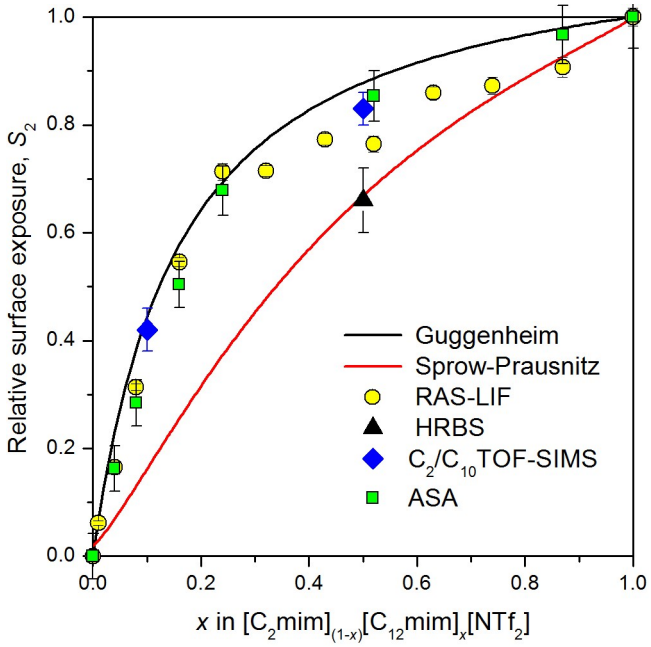

Figure 6. Relative surface exposures of the C12 chains as a function of mole fraction in $[C_2mim]_{(1-x)}[C_{12}mim]_x[NTf_2]$ mixtures as measured in RAS-LIF (yellow points) compared with a HRBS measurement (black triangle) on the same system from reference [29]. Related TOF-SIMS measurements of the $[C_{10}mim][NTf_2]$ surface fraction in $[C_2mim]_{(1-x)}[C_{10}mim]_x[NTf_2]$ mixtures (blue diamonds), from reference [15]. Predictions of the Guggenheim model (black line) and Sprow-Prausnitz equation (red line), based on absolute surface areas as derived by Nakajima et al. in reference [29]. Relative surface densities of secondary hydrogen derived by the surface-wetting analysis of the MD simulations of $[C_2mim]_{(1-x)}[C_{12}mim]_x[NTf_2]$ described in the text (green points).

In their more recent work,[28, 29] Nakajima et al. had introduced an alternative model originally due to Sprow and Prausnitz,[65] which also attempts to relate surface coverage in mixtures to the surface tensions of the pure materials. Following some simplifying assumptions,[29] x_1^s is the implicit solution of

$$\frac{\left(1-x_1^s\right)^n}{x_1^s} = \frac{\left(1-x_1\right)^n}{x_1} \exp\left(\frac{A_1\left(\sigma_1-\sigma_2\right)}{RT}\right) \qquad \textbf{(4)}$$

where A_i is here the molar surface area of component i, $n = A_1/A_2$, and x_2^s can be obtained simply from $x_1^s + x_2^s = 1$. Although, as noted by Nakajima et al,[29] the prediction is not too far from their observed HRBS result at $x = 0.5$, the qualitative behaviour over the full range of x measured in our RAS-LIF experiments is very poorly reproduced by eqn (4). The level of agreement is again not materially changed by modest differences in the surface tension values reported here and elsewhere.

Empirical fitting functions

An alternative approach to describing surface enrichment has been developed by Piñeiro *et al.* based on an extended Langmuir model.[62, 63] It has been applied recently by Lemraski et al. in the fitting of surface-tension data (to which we return below) for related binary ionic-liquid systems, including mixtures of $[C_4mim][NTf_2]$ and $[C_nmim][NTf_2]$ ($n = 1 - 10$).[66] We consider first whether the extended Langmuir expression can provide an adequate fit to our RAS-LIF data. The model is expressed in terms of volume fractions; recast in terms of the variables introduced here, it states that

$$\phi_2^s = \frac{\beta\phi_2}{\left(1+(\beta-1)\phi_2\right)} \qquad \textbf{(5)}$$

where ϕ_2^s (and ϕ_1^s) is the corresponding surface volume fraction; β is an adjustable parameter that expresses the relative surface preference of component 2 relative to 1; and ϕ_1 and ϕ_2, are fractional bulk volumes. Quite strictly, $\phi_1 + \phi_2$, = 1, other than neglecting non-ideality of mixing, which previous studies suggest should be a good approximation for the bulk phase of most IL mixtures.[60, 67] The model is a development from the conventional Langmuir isotherm, with an additional constraint accounting for surface sites that are already occupied (i.e. by adopting a denominator of $1 + (\beta - 1)\phi_2$ rather than $1 + \beta\phi_2$ in eqn (5)).

View Article Online
DOI: 10.1039/C7FD00175D

Although derived from a different starting point, eqn (5) is actually mathematically identical to eqn (3), other than the straightforward transformation of independent variable, with the association $\beta = \exp(-f_2/kT)/\exp(-f_1/kT)$. A fit of eqn (5) to the RAS-LIF data can therefore be regarded as the best description that is possible within either the Guggenheim or basic extended Langmuir models.

The fit of eqn (5) to the $[C_2mim]_{(1-x)}[C_{12}mim]_x[NTf_2]$ RAS-LIF data is shown in Fig. 7(a), for which $\beta = 3.44$. The unconstrained fit is, of course, in slightly better of agreement with experiment than the attempted Guggenheim prediction in Fig. 6. However, it suffers from the same deficiency in the qualitative shape, with compensating slight under and overestimates of the surface exposure for small and large ϕ_2. That this is a general phenomenon, applying also to the other cationic ($[C_8mim]_{(1-x)}[C_8mimF_{13}]_x[NTf_2]$) and anionic ($[C_6mim][NTf_2]_x[BF_4]_{(1-x)}$) mixtures that we have studied by RAS-LIF here, is demonstrated in Figs. 7(b) and (c).

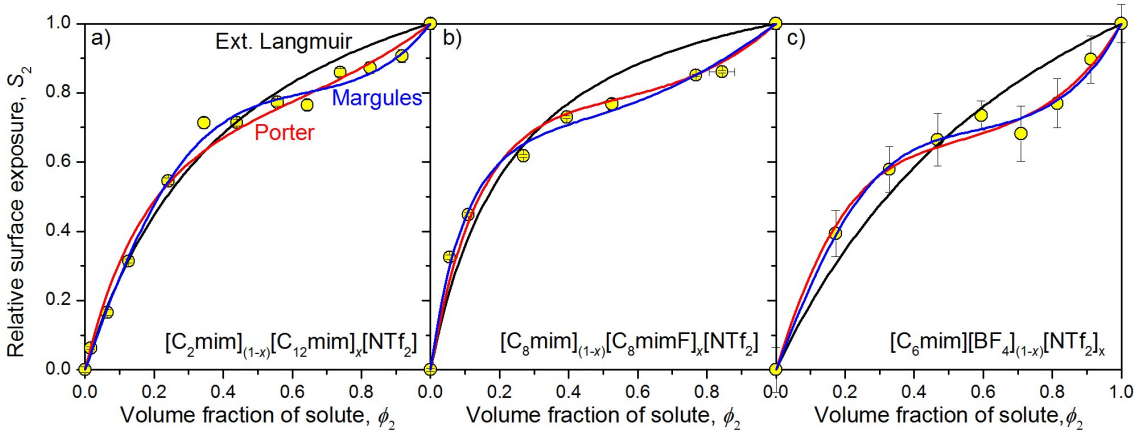

Figure 7. Relative surface exposures measured by RAS-LIF (yellow points) for (a) $[C_2mim]_{(1-x)}[C_{12}mim]_x[NTf_2]$; (b) $[C_8mim]_{(1-x)}[C_8mimF_{13}]_x[NTf_2]$; and (c) $[C_6mim][NTf_2]_x[BF_4]_{(1-x)}$, as a function of volume fraction of the more surface active component, ϕ_2. The fits are of the simple Extended Langmuir model, eqn (5) (black lines), and its further developments described in the text: Porter equation, eqn (7) (red lines); Margules equation, eqn (9) (blue lines).

A natural way to proceed to improve the ability of eqn (5) to describe the RAS-LIF data is to introduce a bulk-composition-dependent activity coefficient, γ_2, that modifies ϕ_2. This is equivalent to modifying the rate of adsorption when constructing the Extended Langmuir isotherm. The simplest approach is to use an expression for γ_2 sometimes known as a Margules equation[68] or elsewhere as the Porter equation (which is the label we adopt),[69] which applies to *regular* solutions (i.e. those for which the entropy of mixing is ideal but the enthalpy of mixing is not). This may be written

$$\ln\gamma_2 = A\phi_1^2 \qquad \textbf{(6)}$$

where A is an empirical parameter. With this modification applied, eqn (5) becomes

$$\phi_2^s = \frac{\beta\phi_2 \exp\left(A(1-\phi_2)^2\right)}{\left(1+(\beta-1)\phi_2 \exp\left(A(1-\phi_2)^2\right)\right)} \qquad \textbf{(7)}$$

Fits of eqn (7) to each of the RAS-LIF data sets are shown in Fig. 7. With the additional adjustable parameter, the fits are not surprisingly considerably improved over the basic eqn (5).

Continuing this logic, higher-order terms can be introduced into the activity coefficient expression to account for deviations from the Porter model. One version of this is also known in some literature[69] as the Margules equation (as we refer to it here):

$$\ln\gamma_2 = \left[A_1 + 2(A_2 - A_1)\phi_2\right]\phi_1^2 \qquad \textbf{(8)}$$

where $A_1 = A + B$ and $A_2 = A - B$. The parameters A and B result from expanding the expression for the excess Gibbs free energy, such that A in eqn (6) becomes $A + B(\phi_1 - \phi_2)$.[69] Introducing eqn (8) into the extended Langmuir model gives the result

$$\phi_2^s = \frac{\beta\phi_2 \exp\left(\left[A_1 + 2(A_2 - A_1)\phi_2\right](1-\phi_2)^2\right)}{\left(1 + (\beta - 1)\phi_2 \exp\left(\left[A_1 + 2(A_2 - A_1)\phi_2\right](1-\phi_2)^2\right)\right)} \qquad \textbf{(9)}$$

View Article Online
DOI: 10.1039/C7FD00175D

The corresponding least-squares fits are also shown in Fig. 7. The overall fit to all three sets of RAS-LIF data is not surprisingly further improved, capturing the Raoult's Law-like behaviour faithfully at high ϕ_2. For the $[C_2mim]_{(1-x)}[C_{12}mim]_x[NTf_2]$mixture on which we focus most attention, the fitted parameters are A_1 = 1.32 ± 0.12, A_2 = 1.92 ± 0.14 and β = 0.77 ± 0.11. Note that the parameter β has a different physical meaning in eqns (7) or (9) from that in eqn (5): at low ϕ_2 in eqn (9), $\phi_2^s = \beta\,\phi_2 \exp(A_1)$. The corresponding limiting Henry's constant for the eqn (9) fit is 2.87 ± 0.53, quite close to that from the basic eqn (5). We conclude that eqn (9) provides a satisfactory phenomenological description of all the mixtures that we have examined so far by RAS-LIF.

Deductions based on composition-dependent surface tensions of mixtures

The predictions using eqns (3) and (4) shown in Fig. 6 appeal only to the surface tensions of the pure components. We consider now how the composition of the surface deduced indirectly from a full set of measured surface tensions as a function of mixing ratio compare to the results that are obtained directly from RAS-LIF (or at sparse points by HRBS).

Following the treatment of Piñeiro and co-workers,[62, 63] Lemraski and Kargar have fitted measured surface tension data for a selection of related ionic liquid mixture systems.[66] They assume that the surface volume fractions obey the extended Langmuir model, eqn (5), with β as an adjustable parameter, as above. A second adjustable parameter, λ, is introduced through the Margules-type expression

$$\sigma = \phi_1^s\sigma_1 + \phi_2^s\sigma_2 - \lambda\phi_1^s\phi_2^s(\sigma_1 - \sigma_2) \qquad \textbf{(10)}$$

The fit is performed in terms of the reduced surface pressure, $\pi^* = \pi/\pi^0$, where the surface pressure, $\pi = \sigma_1 - \sigma$, is normalised to the surface tension difference of the pure components, $\pi^0 = \sigma_1 - \sigma_2$.[62] (Component 1 is taken to be the one with the higher surface tension, and hence lower surface preference, consistent with the labelling above.) The fit is to the expression

$$\pi^* = \frac{\beta(\beta + \alpha(\phi_1/\phi_2))}{(\beta + (\phi_1/\phi_2))^2} \qquad \textbf{(11)}$$

where $\alpha = 1 + \lambda$. We have carried out the fit of eqn (11) to our measured surface tension data for $[C_2mim]_{(1-x)}[C_{12}mim]_x[NTf_2]$ mixtures, with the results shown in Fig. 8 (a). The fit is again reasonable but not perfect; systematic deviations are seen to the low and high side of the experimental data at low and high ϕ_2, respectively. The fitted parameters are α = 1.000±0.067 (implying $\lambda \approx 0$) and β = 2.18±0.15. This implies that the fit is essentially unable to make use of the additional degree of freedom through the term in λ in eqn (10), which allows for non-ideality in the surface tension of mixing of components 1 and 2. The result for β can be reinserted in eqn (5) to generate a *prediction* of the RAS-LIF data, which is shown in Fig. 8(c). This indirect prediction is only modestly poorer than the direct fit of eqn (5) to the RAS-LIF data (see Fig. 7(a), black line, reproduced in Fig 8(c) as a dashed blue line, for ease of comparison). The qualitatively similar systematic deviations of the fits from both the surface tension and RAS-LIF data suggest that the inadequacy rests in some inherent oversimplification in eqn (5).

An alternative approach to extracting the surface composition from measured surface tensions for related ionic liquid mixtures has been described by Oliveira *et al*.[60, 61] Deviations, $\delta\sigma$, from linear behaviour as a function of bulk mole fraction

$$\delta\sigma = \sigma - (x_1\sigma_1 + x_2\sigma_2) \qquad \textbf{(12)}$$

are fit to the Redlich-Kister equation[70]

$$\delta\sigma = x_1x_2\sum_K A_K(x_1 - x_2)^K \qquad \textbf{(13)}$$

where A_K are coefficients and the expansion is performed up to a chosen order. We have carried out the fits of eqn (13) to our measured surface tension data for $[C_2mim]_{(1-x)}[C_{12}mim]_x[NTf_2]$ mixtures. The results of the second-order fit are shown in Fig. 8(b). The fit appears quite plausible, capturing most of the inflexions in the data. There is no statistically significant improvement for higher orders.

View Article Online
DOI: 10.1039/C7FD00175D

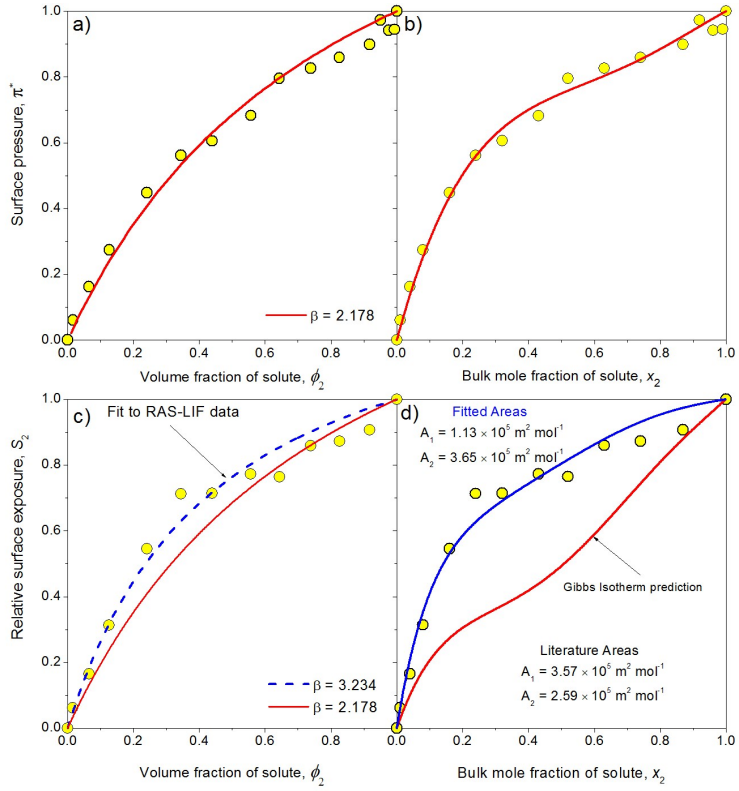

Figure 8. (a) and (b) Reduced surface pressure (yellow points) derived from the surface tension measurements for $[C_2mim]_{(1-x)}[C_{12}mim]_x[NTf_2]$ in Fig. 3 as a function of bulk volume fraction and bulk mole fraction, respectively. (c) and (d) The corresponding surfaces exposures (yellow points) measured via RAS-LIF are shown against the same variables. The fit to surface tension in (a) is of eqn (11)(red line); the corresponding *prediction* of the RAS-LIF data via eqn (5) is shown in (c) (red line), with the direct fit of eqn (5) to the RAS-LIF data (cf Fig. 7(a)) included (dashed blue line) for comparison. The fit to surface tension in (b) is based on eqn (13)(red line); the corresponding *prediction* of the RAS-LIF data via the application of eqns (14) and (16) with predetermined surface areas from reference [29] for each component is shown in (d) (red line). The improved fit of eqn (16) that can be achieved by treating the surface areas of the components as adjustable is also shown in (d) (blue line).

The fitted variation can be used to extract the relative adsorption coefficient (also known as the relative surface excess[71]), $\Gamma_2^{(1)}$, of component 2 with respect to component 1, with an implicit assumption of ideality, via the Gibbs adsorption equation:

$$\Gamma_2^{(1)} = \frac{-1}{RT}\frac{d\sigma}{d\ln x_2} \qquad \textbf{(14)}$$

The relative adsorption coefficients were derived through eqn (14) (analytical and numerical integration give essentially identical results). The results from the 2nd-order versions of eqn (13) are shown in Fig. 8(c); the numerical values of the fitted parameters are given in the ESI. The relative adsorption coefficients are absolute quantities, which are related to the amounts of each component per unit area of surface, n_i^s / A, and to the bulk mole fractions through[71]

$$\frac{n_2^s}{A} = \Gamma_2^{(1)} + \frac{n_1^s}{A}\frac{x_2}{x_1} \qquad \textbf{(15)}$$

If it is assumed that the total surface area is a linear combination of the surface areas of the two components weighted by their amounts per unit area of surface, the desired quantity, n_2^s / A, can be evaluated from

$$\frac{n_2^s}{A} = \frac{\Gamma_2^{(1)} + \frac{1}{A_1^s}\frac{x_2}{x_1}}{1 + \frac{A_2^s}{A_1^s}\frac{x_2}{x_1}} \qquad \textbf{(16)}$$

View Article Online
DOI: 10.1039/C7FD00175D

Our aim is to compare relative values of n_2^s / A to the measured variation in the RAS-LIF signal. Note that this requires values for the molar surface areas of the two components, A_1^s and A_2^s. We adopt the values derived by Nakajima et al through their analysis of HRBS data, introduced above.[29] After normalisation, this generates the results shown in Fig. 8 (d). The prediction of the RAS-LIF data is obviously rather poor. Although the correct sign of the departure from ideality is obtained, the magnitude is seriously underestimated, only approaching the observed values at very low and high mole fractions. Considerably better agreement can be achieved if the surface areas A_1^s and A_2^s are allowed to float in a *fit* of eqn (16) to the RAS-LIF data, with $\Gamma_2^{(1)}$ constrained to the values derived from the surface tension data via eqn (14). This is also illustrated in Fig. 8(d), with details of the fitting procedure in the ESI.

Discussion and comparison with Molecular Dynamics simulations

The main observations that we draw from the analysis of our RAS-LIF results and comparison with the sparse, comparable direct measurements and complementary measurements of surface tension are that:

(1) Essentially all experimental methods agree that the surface has an excess of the component with the lower surface tension, which in the case of the primary example of $[C_2mim]_{(1-x)}[C_{12}mim]_x[NTf_2]$ mixtures equates to $[C_{12}mim][NTf_2]$, but they disagree about the absolute magnitude of the excess and its variation with composition.

(2) Different models are able to capture the qualitative nature of the observed variation of surface excess observed via any single method with varying degrees of success. They essentially all capture quite well the 'Henry's Law' preference at low mole fractions of the more surface active component, but higher-order terms are needed to reproduce the convergence on 'Raoult's Law' behaviour at high *x*.

(3) In attempts to correlate the indirect surface tension measurements with direct RAS-LIF measurements, different approaches give quite different levels of agreement.

The origin of all of these observations is, of course, linked at least in part to what is actually measured in each technique and how this relates to the molecular-level structure of the interface. Insight into this is provided by the MD simulations which we have carried out and reported in part previously,[27] but of which we provide further analysis here.

The MD snapshots represented in side-on view in Fig. 9 show qualitatively the expected presence of an outer layer that is rich in C12 chains, over an underlayer of predominantly headgroups and anions that grows in as the mole fraction of $[C_{12}mim][NTf_2]$ increases. We quantify this further in Fig. 10, which shows the densities of different sites in the cations as a function of distance perpendicular to the interface. This confirms the progressive dominance of the outer layers by the C12 chains.

As has already been widely discussed, different direct physical methods will probe this outer layer to different physical depths, so it is not too surprising that they give different quantitative results.[13-18, 29, 30] Nakajima at al had previously concluded that TOF-SIMS was even more surface sensitive than HRBS,[15] as displayed in Fig. 6. We have good dynamical reasons for believing that RAS-LIF only probes the extreme outer layers,[18] essentially because of the observed minor extent of energy exchange between translational and internal degrees of freedom of the OH product and the liquid surface. Consistently, based on the admittedly limited directly comparable data for $[C_2mim]_{(1-x)}[C_{12}mim]_x[NTf_2]$ mixtures available as a function of mole fraction, RAS-LIF gives somewhat higher surface exposures than HRBS, closer to those from TOF-SIMS. Only an isolated report using ARXPS has suggested an absence of non-stoichiometry surface segregation for related mixed long and short chain systems.[13] However, this may not solely be the result of an intrinsic larger penetration depth for the ARXPS, with the interpretation of the data having been questioned by Nakajima et al.[29] Nakajima et al.'s own HRBS measurements on similar anionic mixtures (but with a different cation),[28] and independent LEIS measurements by Lovelock on related mixed-anion systems,[30] complement our inferred preference here for $[NTf_2]^-$ to dominate the surface of $[C_6mim][NTf_2]_x[BF_4]_{(1-x)}$. There are no prior data as far as we know on the surfaces of mixtures of cations containing alkyl and fluoroalkyl chains and a common anion. Perhaps the closest related work is that of Canongia Lopes and co-workers, who have measured surface tensions and carried out MD simulations for a series of single-component ILs composed of $[C_nmim]^+$ cations of different chain lengths with a common perfluorobutanesulfonate anion.[72] They find that for equal chain lengths, the perfluoro anionic chain predominates at the surface, being increasingly displaced by longer cationic alkyl chains. To the extent that these distinct systems are directly comparable, this is compatible with our observations on $[C_8mim]_{(1-x)}[C_8mimF_{13}]_x[NTf_2]$ mixtures here.

View Article Online
DOI: 10.1039/C7FD00175D

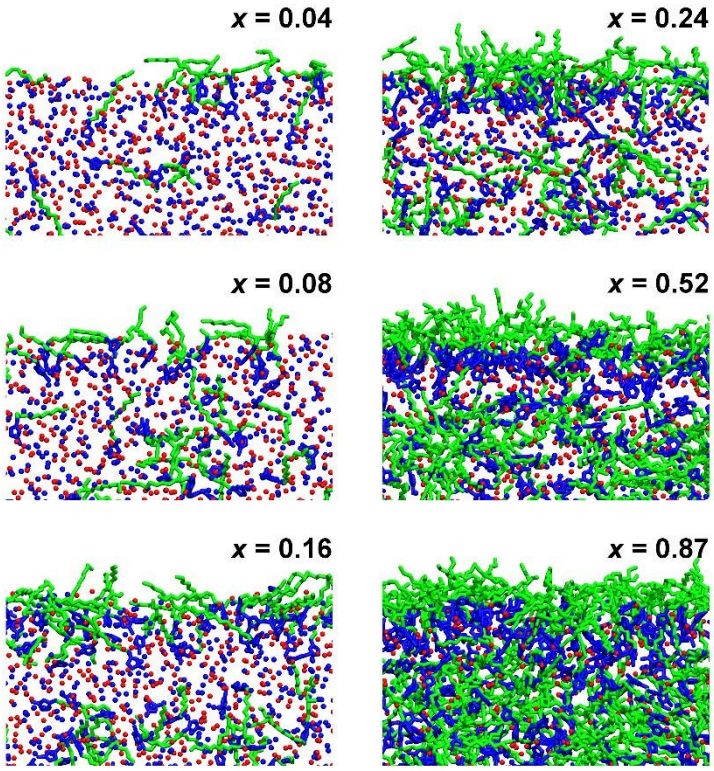

Figure 9. Representative snapshots from MD simulations of $[C_2mim]_{(1-x)}[C_{12}mim]_x[NTf_2]$ mixtures, highlighting the liquid structure at and near the vacuum-liquid interface.. The location of the $[NTf_2]^-$ nitrogen atom is indicated by a red sphere. The location of the unique ring carbon atom in $[C_2mim]^+$ is identified with a blue sphere. The terminal 11 carbon atoms of the $[C_{12}mim]^+$ dodecyl group are rendered as a green tube. The remaining carbon and nitrogen atoms of the $[C_{12}mim]^+$ cation are rendered as a blue tube.

More subtly, Fig. 10 also implies that the $[C_{12}mim]^+$ cations are oriented towards vacuum, because sites further from the N-terminus are found at progressively larger distances on average. The conformation of these surface-active dodecyl chains is further quantified through the probability distributions shown in Fig. 11. This figure plots the probability density distributions, $P(\theta)$ of the angle, θ, between the global surface normal and a vector defined between two carbon atoms in the $[C_{12}mim]^+$ dodecyl group. We identify the vector between C1 and C6 as the "root" and similarly between C7 and C12 as its "tail." Note that these distributions are normalized so that

$$\int P(\theta)\, d\theta = 1 \qquad \textbf{(17)}$$

Fig. 11 demonstrates that the great majority of the C12 chains project outwards from the surface with angles less than 90 degrees from the global surface normal. There is some tendency for the “root” to be more upright, with the “tail” lying flatter and more parallel to the surface plane. This is consistent with similar observations for long-chain pure ILs. However, Fig. 11 also demonstrates that the orientation of the dodecyl group is sensitive to the composition of the $[C_2mim]_{(1-x)}[C_{12}mim]_x[NTf_2]$ mixture. Specifically, the $P(\theta)$ distributions for the "root" and "tail" shift systematically to lower values of θ as the $[C_{12}mim]^+$ mole fraction increases. As shown in Fig. 12, the average angle of the "root" is near 45° at low x and declines to a value near 36° for pure $[C_{12}mim][NTf_2]$.The dodecyl "tail" shows a similar decay from ~60° at x = 0.04 - 0.24 to ~48° at x = 1.

This is relevant to what the RAS-LIF technique measures, because it is ultimately sensitive to the accessibility of the secondary CH_2 units along the alkyl backbone. This will be reduced as the chains become more upright. Our previous work on reactions of $O(^3P)$ with thioalkyl self-assembled monolayers, for example, has shown the reduced overall reactivity of the SAMs due to the preferential exposure of the less-reactive terminal methyl group.[73, 74] Nevertheless, this effect appears to be quite modest for $[C_2mim]_{(1-x)}[C_{12}mim]_x[NTf_2]$ mixtures; our previous ‘surface-wetting’ analysis, described in detail elsewhere,[27] predicts results for alkyl chain accessibility that are in good agreement with the RAS-LIF results. This is illustrated in Fig. 6, where the results of the previous surface-wetting analysis are shown alongside the measured RAS-LIF data.

View Article Online
DOI: 10.1039/C7FD00175D

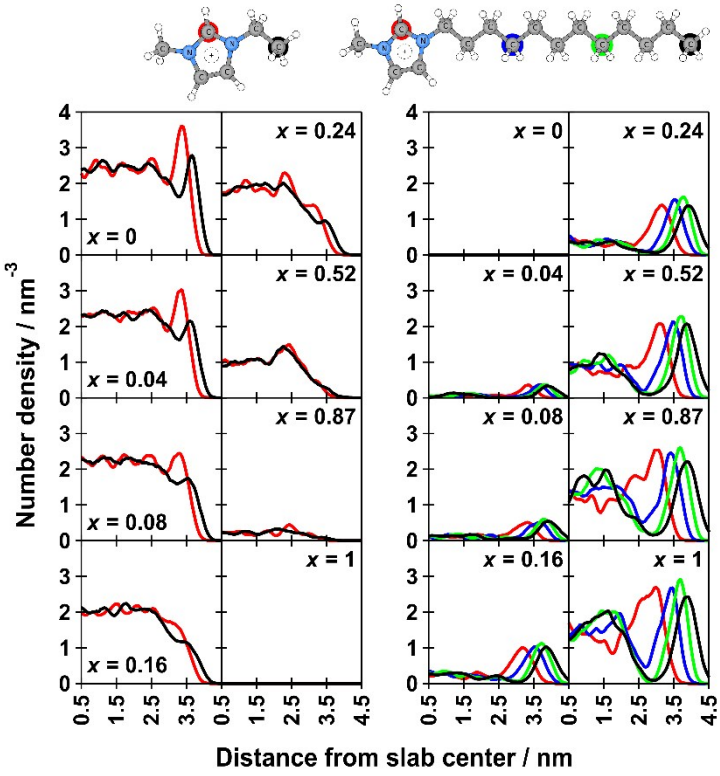

Figure 10. Number density profiles for selected atoms in $[C_2mim]_{(1-x)}[C_{12}mim]_x[NTf_2]$ mixtures. All profiles are computed along the z-axis of the periodic-boundary-condition unit cell (parallel or anti-parallel to the global surface normal for the liquid slab). *Left*: Color-coded number density profiles for selected $[C_2mim]^+$ atoms. *Right*: Color-coded number density profiles for selected $[C_{12}mim]^+$ atoms.

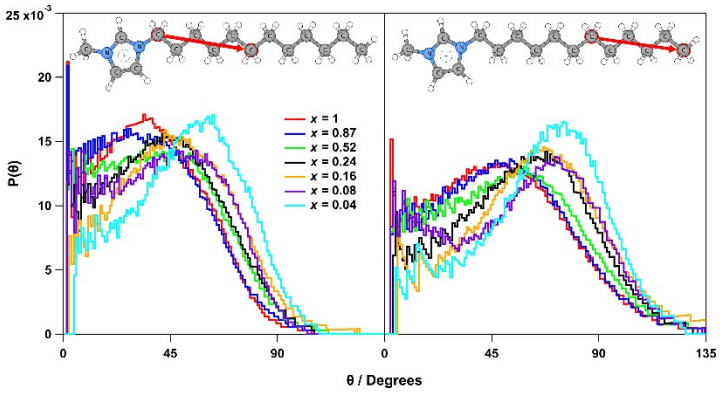

Figure 11. Probability density distributions for the angle, θ, defined between the global surface normal and the indicated vector in $[C_2mim]_{(1-x)}[C_{12}mim]_x[NTf_2]$ mixtures. Contributions beyond θ = 135° are negligible. *Left*: Distributions for the orientation of the dodecyl group "root." *Right*: Distributions for the orientation of the dodecyl group "tail."

We conclude from this that the majority of the observed variation of the RAS-LIF signal as a function of composition is not solely the result of reorganisation of the surface structure as function of mole fraction. In particular, the failure of the simple Extended Langmuir model to describe the data accurately is a real phenomenon. The Extended Langmuir model, expressed in eqn (5), effectively assumes single, fixed surface free energies for each of the components, independent of the mixing ratio. This neglects cooperative effects at either the surface or in the bulk (with which the surface is always ultimately in competition as a site for C12

chains, the chemical potentials of all components being equal, by definition, throughout the system at equilibrium). The model was devised to treat systems where no surface saturation or aggregation were present.[62, 63] There is, however, extensive evidence of bulk aggregation from our X-ray and neutron scattering experiments.[27] A detailed MD analysis of this formation of progressively larger C12-chain aggregates and ultimately inter-percolating polar and non-polar networks is given in our previous work;[27] however, it can be seen qualitatively by examination of the deeper regions in Fig. 9. We suggest that the changing degree of lipophilicity of the bulk accompanying these changes is associated with the need for the activity introduced through eqn (6), and the further improved performance through the non-linear terms in eqn (8) that generates eqn (9).

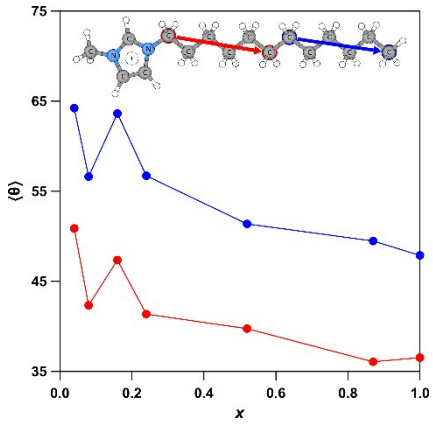

Figure 12. Average value of the angle θ in degrees for the "root" and "tail" of the dodecyl group in $[C_2mim]_{(1-x)}[C_{12}mim]_x[NTf_2]$ mixtures.

The need for these higher-order terms in eqn (8) is again probably not unexpected on general grounds, considering that the regular solutions to which eqn (6) usually applies are mixtures of nonpolar components with similar sizes.[69] We are reassured of the physical reality of these higher-order terms by the fact that eqn (9) is able to reproduce the observed variation for the three quite distinct type of mixtures in Fig. 7. In making the connection to the surface tension data, it is also clear that the basic Extended Langmuir model, eq (5), provides a relatively good single-parameter fit to the surface tension data in Fig. 8(a). Strikingly, this reproduces quite plausibly the RAS-LIF data as shown in Fig. 8(c), but with essentially the same qualitative deviations. We expect that a similar improvement of the fit to surface tension data to that achieved for the RAS-LIF results could be obtained by introducing additional non-linear terms in the relationship between surface and bulk composition. Therefore, despite the fact that surface tension is almost certainly not purely determined by the interactions between alkyl chains in the extreme outer layer and is affected by the cohesive interactions in the polar underlayer, it does appear to give a relatively consistent picture of the composition of the interface. Interestingly, recent simulations of a range of much simpler molecular liquids have suggested that the topmost molecular layer is overwhelmingly responsible for the observed surface tension.[75] We are not aware of such an analysis having been attempted for the more complex case of ionic liquids.

The relatively good consistency between the surface tension and RAS-LIF data that can be achieved via the Extended Langmuir model suggests that this is not in itself the reason why the Sprow-Prausnitz model (Fig. 6), based only on the surface tensions of the pure components, or Gibbs adsorption isotherm (Fig. 8(d)), using the surface tension as a function of the full range of compositions, give relatively poor agreement. Both these approaches depend sensitively on the assumed values of the molar surface areas of each of the components. The independently determined surface areas derived by Nakajima et al. from their HRBS measurements are used in these predictions.[29] These values are $A_1 = 3.57 \times 10^5$ m^2 mol^{-1} and $A_2 = 2.59 \times 10^5$ m^2 mol^{-1} for $[C_2mim][NTf_2]$ and $[C_{12}mim][NTf_2]$, respectively.‡ If they are treated as free parameters in a fit of eqn (16) in the Gibbs adsorption equation approach, the much improved, but still systematically divergent at higher x_2, agreement also shown in Fig. 8(d) is achieved. The corresponding surface areas are $A_1 = 1.13 \times 10^5$ m^2 mol^{-1} and $A_2 = 3.65 \times 10^5$ m^2 mol^{-1}. It is interesting that the HRBS-derived surface area for $[C_2mim][NTf_2]$ is (counter-intuitively) higher than that for $[C_{12}mim][NTf_2]$, which is reversed in the best-fit values. Moreover, the poor predictions of either the Sprow-Prausnitz or Gibbs adsorption equations could also potentially reflect unrealistic underlying physical assumptions made in these approaches. The Gibbs adsorption equation, eqn (14) is based on an assumption of ideality, which we have demonstrated here through the direct fits to the RAS-LIF data not to be secure in these systems. The particular version of Sprow-Prausnitz invoked through eqn (4) assumes that partial molar areas are the same as the molar areas in the pure compounds; this may also be called into question by our MD simulations suggesting that the average orientation of chains, and hence fraction of the surface covered per molecule, varies with composition.

Conclusions

View Article Online DOI: 10.1039/C7FD00175D

The surfaces of ionic liquid mixtures are quite generally non-stoichiometrically dominated by the component with lower surface tension. This is demonstrated quantitatively here for a range of imidazolium-based ionic liquid mixtures consisting of mixed cations with long ($[C_{12}mim]^+$) and short chains ($[C_2mim]^+$); mixed cations with hydrogenated ($[C_8mim]^+$) and fluoroalkyl ($[C_8mimF_{13}]^+$) chains of the same length; and mixed anions of different volume ($[BF_4]^-$ and $[NTf_2]^-$).

At low mole fraction of the more surface-active component, direct RAS-LIF measurements of surface composition are well described as a simple relative energetic preference for the surface, analogous to Henry's Law. The Extended Langmuir model provides a satisfactory single-parameter description in this regime. At higher mole fractions, additional non-linear terms are needed to give wholly satisfactory fits to the data, including the asymptotic return towards stoichiometric, Raoult's Law-like, behaviour.

MD simulations support the conclusion that this non-linearity is not an artefact of the RAS-LIF method. They suggest that RAS-LIF faithfully reports on the exposure of alkyl chains at the surface of $[C_2mim]_{(1-x)}[C_{12}mim]_x[NTf_2]$ mixtures. The C12 chains project overwhelmingly into vacuum and their degree of exposure is only subtly modified by composition-dependent structural reorganisation.

Essentially the same systematic composition-dependent deviations from ideality are apparent in the measured surface tensions of $[C_2mim]_{(1-x)}[C_{12}mim]_x[NTf_2]$ mixtures. Fits to surface tension based on the single-parameter Extended Langmuir model are of similar quality to those to the RAS-LIF data and imply quantitatively consistent surface compositions. We conclude that the surface tension must have a dominant contribution from the topmost *molecular* layer, consisting of the non-polar overlayer of C12 chains and polar underlayer of imidazolium headgroups (to some of which the C12 chains are, by construction, attached) and counterions, identified clearly in MD simulations.

However, analyses of surface tension data based on either the Sprow-Prausnitz model or the Gibbs Adsorption equation give much larger discrepancies with direct RAS-LIF measurements. Both these approaches suffer from the need to know the surface areas occupied by each component accurately, but may also rely on over-simplified physical assumptions.

Acknowledgements

The authors acknowledge financial support from NSF and EPSRC (grant numbers NSF-CHE-1266032 and EP/K032062/1, EP/P001459/1), the University of York, Heriot-Watt University, and Montana State University.

We are also grateful to Professor George Schatz, Northwestern University, for helpful discussions and other input into the project. All data created during this research are available by request from the Heriot-Watt University data repository.

Notes and references

‡ Note that these values are derived from the quoted areal atomic densities, d_i, in reference [29] using the prescribed relationship $A_i = N_A N_i / d_i$, where N_i is the number of atoms per ion pair. The molar surface areas listed in Table 1 of reference [29] appear to be too large by a factor of N_i.

1. T. Welton, *Chem. Rev.*, 1999, **99**, 2071-2083.
2. V. I. Parvulescu and C. Hardacre, *Chem. Rev.*, 2007, **107**, 2615-2665.
3. J. P. Hallett and T. Welton, *Chem. Rev.*, 2011, **111**, 3508-3576.
4. N. V. Plechkova and K. R. Seddon, *Chem. Soc. Rev.*, 2008, **37**, 123-150.
5. M. Ramdin, T. W. de Loos and T. J. H. Vlugt, *Industrial & Engineering Chemistry Research*, 2012, **51**, 8149-8177.
6. C. M. Wang, X. Y. Luo, X. Zhu, G. K. Cui, D. E. Jiang, D. S. Deng, H. R. Li and S. Dai, *Rsc Advances*, 2013, **3**, 15518-15527.
7. D. B. Zhao, M. Wu, Y. Kou and E. Min, *Catal. Today*, 2002, **74**, 157-189.
8. T. Welton, *Coord. Chem. Rev.*, 2004, **248**, 2459-2477.
9. Q. Zhang, S. Zhang and Y. Deng, *Green Chemistry*, 2011, **13**, 2619-2637.
10. H. P. Steinruck and P. Wasserscheid, *Catal. Lett.*, 2015, **145**, 380-397.
11. R. Hayes, G. G. Warr and R. Atkin, *Chem. Rev.*, 2015, **115**, 6357-6426.
12. M. Tariq, M. G. Freire, B. Saramago, J. A. P. Coutinho, J. N. C. Lopes and L. P. N. Rebelo, *Chem. Soc. Rev.*, 2012, **41**, 829-868.
13. F. Maier, T. Cremer, C. Kolbeck, K. R. J. Lovelock, N. Paape, P. S. Schulz, P. Wasserscheidc and H. P. Steinruck, *PCCP*, 2010, **12**, 1905-1915.
14. H. P. Steinruck, *Surf. Sci.*, 2010, **604**, 481-484.
15. K. Nakajima, M. Miyashita, M. Suzuki and K. Kimura, *J. Chem. Phys.*, 2013, **139**, 224701.

16. I. J. Villar-Garcia, S. Fearn, G. F. De Gregorio, N. L. Ismail, F. J. V. Gschwend, A. J. S. McIntosh and K. R. J. Lovelock, *Chem Sci*, 2014, **5**, 4404-4418.
17. C. S. Santos and S. Baldelli, *Chem. Soc. Rev.*, 2010, **39**, 2136-2145.
18. M. A. Tesa-Serrate, E. J. Smoll, T. K. Minton and K. G. McKendrick, *Annu. Rev. Phys. Chem.*, 2016, **67**, 515-540.
19. B. H. Wu, J. M. Zhang, T. K. Minton, K. G. McKendrick, J. M. Slattery, S. Yockel and G. C. Schatz, *J. Phys. Chem. C*, 2010, **114**, 4015-4027.
20. C. Waring, P. A. J. Bagot, J. M. Slattery, M. L. Costen and K. G. McKendrick, *J Phys Chem Lett*, 2010, **1**, 429-433.
21. C. Waring, P. A. J. Bagot, J. M. Slattery, M. L. Costen and K. G. McKendrick, *J. Phys. Chem. A*, 2010, **114**, 4896-4904.
22. C. Waring, P. A. J. Bagot, M. L. Costen and K. G. McKendrick, *J Phys Chem Lett*, 2011, **2**, 12-18.
23. M. A. Tesa-Serrate, B. C. Marshall, E. J. Smoll, S. M. Purcell, M. L. Costen, J. M. Slattery, T. K. Minton and K. G. McKendrick, *J. Phys. Chem. C*, 2015, **119**, 5491-5505.
24. M. A. Tesa-Serrate, E. J. Smoll, L. D'Andrea, S. M. Purcell, M. L. Costen, D. W. Bruce, J. M. Slattery, T. K. Minton and K. G. McKendrick, *J. Phys. Chem. C*, 2016, **120**, 27369-27379.
25. B. C. Marshall, E. J. Smoll, S. M. Purcell, M. L. Costen, K. G. McKendrick and T. K. Minton, *J. Phys. Chem. C*, 2016, **120**, 12472-12483.
26. S. M. Purcell, M. A. Tesa-Serrate, B. C. Marshall, D. W. Bruce, L. D'Andrea, M. L. Costen, J. M. Slattery, E. J. Smoll, T. K. Minton and K. G. McKendrick, *Langmuir*, 2016, **32**, 9938-9949.
27. D. W. Bruce, C. P. Cabry, J. Nuno Canongia Lopes, M. L. Costen, L. D'Andrea, I. Grillo, B. C. Marshall, K. G. McKendrick, T. K. Minton, S. M. Purcell, S. E. Rogers, J. M. Slattery, K. Shimizu, E. Smoll and M. A. Tesa-Serrate, *J. Phys. Chem. B*, 2017, DOI: 10.1021/acs.jpcb.7b01654.
28. K. Nakajima, S. Nakanishi, Z. Chval, M. Lisal and K. Kimura, *J. Chem. Phys.*, 2016, **145**, 184704.
29. K. Nakajima, S. Nakanishi, M. Lisal and K. Kimura, *J. Mol. Liq.*, 2017, **230**, 542-549.
30. I. J. Villar-Garcia, S. Fearn, N. L. Ismail, A. J. S. McIntosh and K. R. J. Lovelock, *Chem. Commun.*, 2015, **51**, 5367-5370.
31. R. P. Baker, M. L. Costen, G. Hancock, G. A. D. Ritchie and D. Summerdeld, *PCCP*, 2000, **2**, 661-664.
32. D. J. Garton, T. K. Minton, M. Alagia, N. Balucani, P. Casavecchia and G. Gualberto Volpi, *Faraday Discuss.*, 1997, **108**, 387-399.
33. J. Zhang, D. J. Garton and T. K. Minton, *J. Chem. Phys.*, 2002, **117**, 6239-6251.
34. J. Zhang, H. P. Upadhyaya, A. L. Brunsvold and T. K. Minton, *J. Phys. Chem. B*, 2006, **110**, 12500-12511.
35. H. Kelso, S. P. K. Köhler, D. A. Henderson and K. G. McKendrick, *J. Chem. Phys.*, 2003, **119**, 9985-9988.
36. S. P. K. Köhler, M. Allan, H. Kelso, D. A. Henderson and K. G. McKendrick, *J. Chem. Phys.*, 2004, **122**, 024712.
37. S. P. K. Köhler, M. Allan, M. L. Costen and K. G. McKendrick, *J. Phys. Chem. B*, 2006, **110**, 2771-2776.
38. S. P. K. Köhler, S. K. Reed, R. E. Westacott and K. G. McKendrick, *J. Phys. Chem. B*, 2006, **110**, 11717-11724.
39. M. Allan, P. A. J. Bagot, M. L. Costen and K. G. McKendrick, *J. Phys. Chem. C*, 2007, **111**, 14833-14842.
40. M. Allan, P. A. J. Bagot, S. P. K. Köhler, K. R. Stewart, R. E. Westacott, M. L. Costen and K. G. McKendrick, *Phys. Scr.*, 2007, **76**, C42.
41. M. J. Abraham, T. Murtola, R. Schulz, S. Páll, J. C. Smith, B. Hess and E. Lindahl, *SoftwareX*, 2015, **1–2**, 19-25.
42. A. A. H. Pádua, *J. Phys. Chem. A*, 2002, **106**, 10116-10123.
43. J. N. Canongia Lopes, J. Deschamps and A. A. H. Pádua, *J. Phys. Chem. B*, 2004, **108**, 2038-2047.
44. J. N. C. Lopes, J. Deschamps and A. A. H. Padua, *J. Phys. Chem. B*, 2004, **108**, 11250-11250.
45. J. N. Canongia Lopes and A. A. H. Pádua, *J. Phys. Chem. B*, 2004, **108**, 16893-16898.
46. J. N. Canongia Lopes and A. A. H. Pádua, *J. Phys. Chem. B*, 2006, **110**, 19586-19592.
47. J. N. Canongia Lopes, A. A. H. Pádua and K. Shimizu, *J. Phys. Chem. B*, 2008, **112**, 5039-5046.
48. K. Shimizu, D. Almantariotis, M. F. C. Gomes, A. A. H. Pádua and J. N. Canongia Lopes, *J. Phys. Chem. B*, 2010, **114**, 3592-3600.
49. W. L. Jorgensen, D. S. Maxwell and J. Tirado-Rives, *J. Am. Chem. Soc.*, 1996, **118**, 11225-11236.
50. W. L. Jorgensen and N. A. McDonald, *Journal of Molecular Structure: THEOCHEM*, 1998, **424**, 145-155.
51. G. Kaminski and W. L. Jorgensen, *J. Phys. Chem.*, 1996, **100**, 18010-18013.
52. G. A. Kaminski, R. A. Friesner, J. Tirado-Rives and W. L. Jorgensen, *J. Phys. Chem. B*, 2001, **105**, 6474-6487.
53. N. A. McDonald and W. L. Jorgensen, *J. Phys. Chem. B*, 1998, **102**, 8049-8059.
54. M. L. P. Price, D. Ostrovsky and W. L. Jorgensen, *J. Comput. Chem.*, 2001, **22**, 1340-1352.
55. R. C. Rizzo and W. L. Jorgensen, *J. Am. Chem. Soc.*, 1999, **121**, 4827-4836.
56. E. K. Watkins and W. L. Jorgensen, *J. Phys. Chem. A*, 2001, **105**, 4118-4125.
57. G. Bussi, D. Donadio and M. Parrinello, *J. Chem. Phys.*, 2007, **126**, 014101.
58. A. Muhammad, M. I. A. Mutalib, C. D. Wilfred, T. Murugesan and A. Shafeeq, *J. Chem. Thermodyn.*, 2008, **40**, 1433-1438.
59. C. Kolbeck, J. Lehmann, K. R. J. Lovelock, T. Cremer, N. Paape, P. Wasserscheid, A. P. Froba, F. Maier and H. P. Steinruck, *J. Phys. Chem. B*, 2010, **114**, 17025-17036.
60. M. B. Oliveira, M. Dominguez-Perez, M. G. Freire, F. Llovell, O. Cabeza, J. A. Lopes-da-Silva, L. F. Vega and J. A. P. Coutinho, *J. Phys. Chem. B*, 2012, **116**, 12133-12141.
61. M. B. Oliveira, M. Dominguez-Perez, O. Cabeza, J. A. Lopes-da-Silva, M. G. Freire and J. A. P. Coutinho, *J. Chem. Thermodyn.*, 2013, **64**, 22-27.
62. Á. Piñeiro, P. Brocos, A. Amigo, J. Gracia-Fadrique and M. Guadalupe Lemus, *Langmuir*, 2001, **17**, 4261-4266.
63. P. Brocos, J. Gracia-Fadrique, A. Amigo and Á. Piñeiro, *Fluid Phase Equilib.*, 2005, **237**, 140-151.
64. E. A. Guggenheim, *T Faraday Soc*, 1945, **41**, 150-156.
65. F. B. Sprow and J. M. Prausnitz, *T Faraday Soc*, 1966, **62**, 1105-1111.
66. E. G. Lemraski and E. Kargar, *J. Mol. Liq.*, 2014, **195**, 17-21.

67. J. N. C. Lopes, T. C. Cordeiro, J. M. S. S. Esperanca, H. J. R. Guedes, S. Huq, L. P. N. Rebelo and K. R. Seddon, *J. Phys. Chem. B*, 2005, **109**, 3519-3525.
68. P. Atkins and J. de Paula, *Physical Chemistry*, Oxford University Press, Oxford, 8th edn., 2006.
69. J. P. O'Connell and J. M. Haile, *Thermodynamics: Fundamentals for Applications*, Cambridge University Press, Cambridge, 2005.
70. O. Redlich and A. T. Kister, *Ind. Eng. Chem.*, 1948, **40**, 341-345.
71. I. N. Levine, *Physical Chemistry*, McGraw-Hill, New York, 5th edn., 2002.
72. A. Luis, K. Shimizu, J. M. M. Araujo, P. J. Carvalho, J. A. Lopes-da-Silva, J. N. C. Lopes, L. P. N. Rebelo, J. A. P. Coutinho, M. G. Freire and A. B. Pereiro, *Langmuir*, 2016, **32**, 6130-6139.
73. C. Waring, P. A. J. Bagot, M. T. Raisanen, M. L. Costen and K. G. McKendrick, *J. Phys. Chem. A*, 2009, **113**, 4320-4329.
74. C. Waring, P. A. J. Bagot, M. W. P. Bebbington, M. T. Raisanen, M. Buck, M. L. Costen and K. G. McKendrick, *J Phys Chem Lett*, 2010, **1**, 1917-1921.
75. M. Sega, B. Fábián, G. Horvai and P. Jedlovszky, *J. Phys. Chem. C*, 2016, **120**, 27468-27477.